

Optical correlation using gated localized holography

Arash Karbaschi
Omid Momtahan

Ali Adibi, MEMBER SPIE
Georgia Institute of Technology
School of Electrical and
Computer Engineering
777 Atlantic Drive NW
Atlanta, Georgia 30332-0250
E-mail: arash@ece.gatech.edu

Bahram Javidi, FELLOW SPIE
University of Connecticut
Department of Electrical and
Computer Engineering
371 Fairfield Road, Unit 1157
Storrs, Connecticut 06269-1157

Abstract. We present a new technique for optical correlation using gated holographic recording by which the holograms are localized in separate slices along the recording medium. We compare the performance of localized holographic correlators (LHCs) with that of the conventional correlators using normal volume holography. Crosstalk, shift invariance, and the capacities of the LHC and of the conventional method are examined. We show that the proposed method has better performance and distinctive advantages over the conventional method. These advantages include selective recording and erasure for dynamic pattern modification, extendable capacity, and compactness. © 2005 Society of Photo-Optical Instrumentation Engineers. [DOI: 10.1117/1.2032227]

Subject terms: holography; pattern recognition; correlators; holography applications.

Paper 040481R received Jul. 19, 2004; revised manuscript received Dec. 24, 2004; accepted for publication Feb. 24, 2005; published online Aug. 23, 2005.

1 Introduction

Optical pattern recognition has been appreciated since the complex spatial filtering work by VanderLugt¹ in 1964 and demonstration of the joint transform correlator by Weaver and Goodman² in 1966. These methods of optical correlation in fact were invented to provide a tool for 2-D spatial filtering. In both of these approaches, only one stored pattern was correlated with the incoming patterns. The advantage of multiplexing several patterns in a volume hologram³ makes optical correlation a significant method to be utilized in optical pattern recognition. In this way, the incoming pattern is correlated with all of the stored patterns, each recorded as a volume hologram. As a result, holographic information processors have massive parallelism and high speed.⁴

Much research has been performed in volume holographic correlation, extending its outstanding capabilities to a variety of applications. Some examples are the implementation of optical neural networks,⁵ real-time vehicle navigation,⁶ content-addressable data,⁷ and fingerprint recognition.⁸ In all these applications, the optical correlation is performed using multiplexed volume holograms, and all of the stored holograms in the system use the whole volume of the recording medium. Since all the stored patterns (or holograms) overlap in the same volume of the recording medium, they must be recorded once all of the patterns are available. Adding extra patterns to or erasing selected patterns from the system after the recording phase is complicated because all of the stored patterns in the recording medium are affected by the optical beams required for recording or erasing some holograms. Thus, the conventional techniques can not be used for dynamic pattern recognition.

In this paper, we introduce the localized holographic correlators (LHCs), which use the localized holographic recording technique⁹ enabled by gated holographic recording in photorefractive crystals.¹⁰ Using this method, every pattern in the system can be recorded and erased at any arbitrary time without affecting other holograms, making LHCs excellent candidates for the implementation of dynamic optical correlators. By simulation, we show that the performance of the LHC measured by crosstalk, shift invariance, and capacity is better than that of the conventional angle-multiplexed optical correlators. Moreover, the capacity of the proposed LHC is extendable by elongation of the recording medium, and the complete correlation system is more compact than a conventional volume holographic correlator.

We explain the basic structure of the LHCs in Sec. 2. Section 3 discusses a theoretical analysis of the performance of LHCs. The performance measures of the LHC are calculated and then compared with those of the conventional correlators in Sec. 4. Section 5 discusses further extension of the capabilities of the LHCs. Section 6 presents final conclusions.

2 LHCs

The basic idea for an LHC is shown in Fig. 1. Figure 1(a) shows the general recording setup for localized holographic recording in 90-deg geometry.¹¹ Each hologram is recorded by the simultaneous overlap of a sensitizing (or gating) beam and two coherent recording beams (i.e., reference beam and signal beam) in a thin slice of the recording medium. Note that different holograms are recorded in different slices and will not overlap with each other. In the recognition phase, the signal beam corresponding to the unknown pattern is correlated with all the stored patterns, as depicted in Fig. 1(b). The unknown pattern will read all the holograms, resulting in diffraction of their correspond-

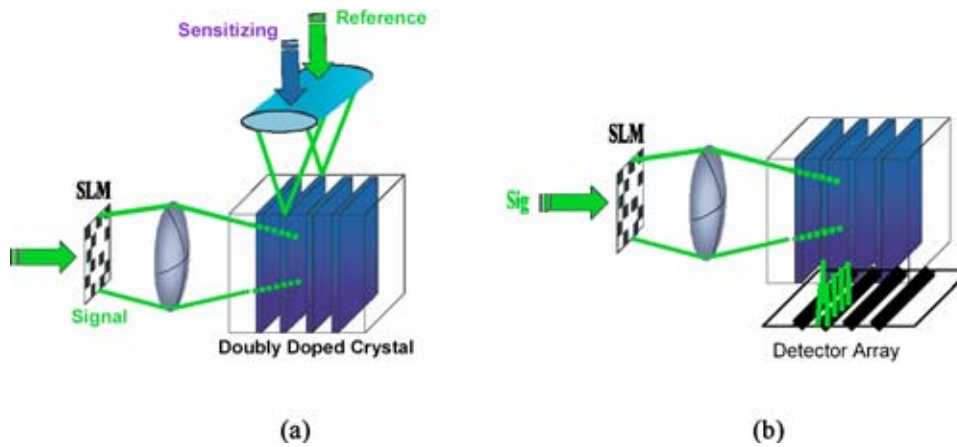


Fig. 1 Localized holographic correlation steps: (a) recording and (b) correlating. During recording, each pattern is recorded as a volume hologram in a thin slice of the recording medium that is sensitized by the sensitizing beam. Reading of a hologram by its corresponding reading beam (or pattern) results in a strong diffracted beam from a thin slice of the recording medium.

ing reference beams, if Bragg matching occurs (i.e., if any of the holograms are read with an optical beam with the same spatial profile used for their recording). The diffracted signals are detected by a detector array adjacent to the recording medium, as shown in Fig. 1(b). If the reading pattern is similar to one of the recorded patterns, a strong diffracted signal is obtained at the detector, corresponding to that pattern. Otherwise, all detected signals are weak, confirming negligible correlation between the reading pattern and all recorded patterns.

The implementation of localized holographic recording is made possible by advances in gated holography techniques: two-step recording¹² and two-center recording.¹³ The latter method, however, has major advantages in a variety of aspects such as sensitivity, dynamic range, and dark storage time.^{10,14} By using gated holography, the recording and erasure of the holograms is possible only in the presence of a (third) sensitizing beam, which acts as a gate. The regions of the recording medium illuminated by the sensitizing (or gating) beam get sensitized so that the two recording beams can record a hologram in those regions. Therefore, by shaping the sensitizing beam to form a thin slice within the recording medium [as shown in Fig. 1(a)], the hologram is localized within the volume of that slice. Since the recording beams affect only the sensitized slice, recording at one slice does not erase holograms previously stored at other slices. As a result, individual patterns can be dynamically inserted into and/or removed from the optical pattern recognition system without affecting the already recorded patterns. Moreover, reading the holograms with the signal beams, in the absence of the sensitizing beam, does not erase the recorded holograms as it does in the conventional (nongated) holography. This gives persistence to the recorded patterns (unless they are erased deliberately by light at the sensitizing wavelength), and prevents the reading beam from being absorbed by the crystal. As a result, the absorption of the reading beam by the holographic medium is negligible and the recording medium can be made long enough to include all the desired patterns.

3 Theoretical Analysis of LHCs

In Fig. 2, the correlation system is illustrated with more details that are used in our analysis. The recording and reading patterns are applied to a spatial light modulator (SLM), which is put in the front focal plane of a lens with focal length F . The SLM is illuminated by a monochromatic plane wave light source at recording wavelength λ . The electromagnetic (EM) field pattern at (u, v, z) within the recording slice, represented by $F_1(u, v, z)$, caused by the recording pattern $f_1(\xi_1, \eta_1)$ at the SLM can be calculated using Fresnel diffraction approximation (see the appendix) as

$$F_1(u, v, z) \propto \int \int_{\text{SLM}} f_1(\xi_1, \eta_1) \times \exp \left[-j \frac{\pi z}{n \lambda F^2} (\xi_1^2 + \eta_1^2) \right] \exp \left(j \frac{2 \pi n z}{\lambda} \right) \times \exp \left[-j \frac{2 \pi}{\lambda F} (u \xi_1 + v \eta_1) \right] d \xi_1 d \eta_1. \quad (1)$$

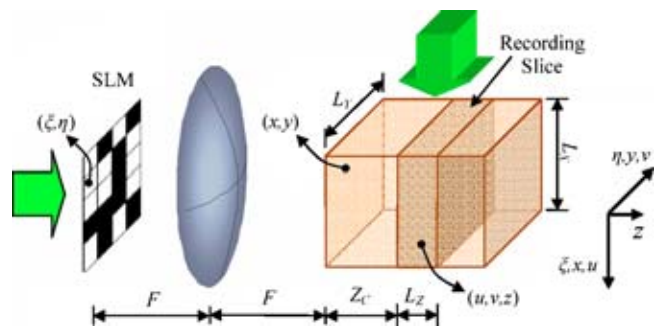


Fig. 2 Basic structure of an LHC. The recorded slice has dimensions L_x , L_y , and L_z in the x , y , and z directions, respectively. The coordinates of the points in the SLM plane, the back focal plane of the lens, and the slice volume are represented by (ξ, η) , (x, y) , and (u, v, z) , respectively. The recorded slice is located at distance Z_c from the back focal plane of the lens ($z=0$) with focal length F .

Here $F_1(u, v, z)$ can represent electric or magnetic field depending on the polarization of the signal beam. All parameters in Eq. (1) are defined in the caption for Fig. 2. The reference beam within the sensitized slice of the recording medium can be approximately represented as a plane wave, i.e., $\exp(jk_u u)$, where $k_u = 2n\pi/\lambda$ with n being the refractive index of the recording material. Therefore the permittivity modulation due to the interference of the signal beam and the reference beam can be represented as

$$\Delta\varepsilon \propto |\exp(jk_u u) + F_1(u, v, z)|^2. \quad (2)$$

Note that the proportionality constant in Eq. (2) depends on the electro-optic properties and the dynamics of the photo-refractive effect of the two-center recording material¹³ and is not included here for simplicity. Expanding Eq. (2), the only component that can produce a Bragg matched diffracted beam during reading by the same pattern at the SLM [i.e., $f_1(\xi, \eta)$] is

$$\Delta\varepsilon_1 \propto F_1^*(u, v, z) \exp(jk_u u). \quad (3)$$

The hologram is then read by another pattern, $f_2(\xi_2, \eta_2)$ at the SLM plane. The reading field pattern at the recorded slice is calculated similar to the recording field pattern [i.e., Eq. (1)] to be

$$\begin{aligned} F_2(u, v, z) \propto & \int \int_{\text{SLM}} f_2(\xi_2, \eta_2) \\ & \times \exp\left[-j\frac{\pi z}{n\lambda F^2}(\xi_2^2 + \eta_2^2)\right] \exp\left(j\frac{2\pi n z}{\lambda}\right) \\ & \times \exp\left[-j\frac{2\pi}{\lambda F}(u\xi_2 + v\eta_2)\right] d\xi_2 d\eta_2. \end{aligned} \quad (4)$$

The diffracted field in wave vector space [represented by $A_d(\mathbf{k}_d)$] is calculated by using Eqs. (2)–(4) and the Born approximation¹⁵

$$A_d(\mathbf{k}_d) \propto \frac{\int \int \int_{\text{Volume}} F_1^*(u, v, z) \exp(jk_u u) F_2(u, v, z) \exp(-j\mathbf{k}_d \cdot \mathbf{r}) du dv dz}{[(2n\pi/\lambda)^2 - k_{dy}^2 - k_{dz}^2]^{1/2}}, \quad (5)$$

where $\mathbf{r} = ua_x + va_y + za_z$ [where a_x , a_y , and a_z are unit vectors in the x , y (or u , v), and z directions, respectively] and \mathbf{k}_d represents the diffracted wave vector with magnitude $|\mathbf{k}_d| = |k_{dx}a_x + k_{dy}a_y + k_{dz}a_z| = 2n\pi/\lambda$. Note that the integral in Eq. (5) is performed over the volume of the recording slice. Assuming $A_d(\mathbf{k}_d)$ to be significant only for k_{dy} , $k_{dz} \ll 2n\pi/\lambda$ (i.e., paraxial approximation for a plane wave in the a_x direction), we neglect k_{dy} and k_{dz} in the denominator of Eq. (5) to obtain

$$\begin{aligned} A_d(\mathbf{k}_d) \propto & \int \int_{\text{SLM}} f_1^*(\xi_1, \eta_1) d\xi_1 d\eta_1 \\ & \times \int \int_{\text{SLM}} f_2(\xi_2, \eta_2) d\xi_2 d\eta_2 \\ & \times \int \int \int_{\text{volume}} \exp\left\{j\left[\frac{2\pi}{\lambda F}\right.\right. \\ & \left.\left. \times (\xi_1 - \xi_2) + \frac{2\pi n}{\lambda} - k_{dx}\right]u\right\} \\ & \times \exp\left\{j\left[\frac{2\pi}{\lambda F}(\eta_1 - \eta_2) - k_{dy}\right]v\right\} \\ & \times \exp\left\{j\left[\frac{2\pi}{n\lambda F^2}(\xi_1^2\right.\right. \\ & \left.\left. + \eta_1^2 - \xi_2^2 - \eta_2^2) - k_{dz}\right]z\right\} du dv dz. \end{aligned} \quad (6)$$

Performing the integral over the volume of the slice yields

$$\begin{aligned} A_d(\mathbf{k}_d) \propto & L_x L_y L_z \int \int_{\text{SLM}} f_1^*(\xi_1, \eta_1) d\xi_1 d\eta_1 \\ & \times \int \int_{\text{SLM}} f_2(\xi_2, \eta_2) d\xi_2 d\eta_2 \times \text{sinc} \\ & \times \left\{ \frac{L_x}{2\pi} \left[\frac{2\pi}{\lambda F}(\xi_1 - \xi_2) + \frac{2\pi n}{\lambda} - k_{dx} \right] \right\} \\ & \times \text{sinc} \left\{ \frac{L_y}{2\pi} \left[\frac{2\pi}{\lambda F}(\eta_1 - \eta_2) - k_{dy} \right] \right\} \\ & \times \text{sinc} \left\{ \frac{L_z}{2\pi} \left[\frac{\pi}{n\lambda F^2}(\xi_1^2 + \eta_1^2 - \xi_2^2 - \eta_2^2) - k_{dz} \right] \right\} \\ & \times \exp\left\{-j\left(Z_C + \frac{L_z}{2}\right)\left[\frac{\pi}{n\lambda F^2}\right.\right. \\ & \left.\left. \times (\xi_1^2 + \eta_1^2 - \xi_2^2 - \eta_2^2) - k_{dz}\right]\right\}, \end{aligned} \quad (7)$$

with $\text{sinc}(x) = \sin(\pi x)/\pi x$. In the following steps, we assume the dimension of the slice in y (or v) direction (i.e., L_y) to be large enough to approximate the second sinc function in Eq. (6) as an impulse (or delta) function. Integration over η_2 then yields

$$\begin{aligned}
 A_d(\mathbf{k}_d) &\propto L_X L_Z \int \int_{\text{SLM}} f_1^*(\xi_1, \eta_1) d\xi_1 d\eta_1 \\
 &\times \int_{\text{SLM}-\xi} f_2(\xi_2, \eta_1 + \Delta\eta) d\xi_2 \\
 &\times \text{sinc} \left[\frac{L_X}{2\pi} \left[\frac{2\pi}{\lambda F} (\xi_1 - \xi_2) + k_x - k_{dx} \right] \right] \\
 &\times \text{sinc} \left(\frac{L_Z}{2\pi} \alpha \right) \exp \left[-j \left(Z_C + \frac{L_Z}{2} \right) \alpha \right], \quad (8)
 \end{aligned}$$

where

$$\alpha = \frac{\pi}{n\lambda F^2} (\xi_1^2 - \xi_2^2 - 2\eta_1 \Delta\eta - \Delta\eta^2) - k_{dz}, \quad (9)$$

$$\Delta\eta = -\frac{\lambda F}{2\pi} k_{dy}, \quad (10)$$

and SLM- ξ means the ξ direction (or x direction) in the SLM plane.

The detector array is located right below the bottom face of the crystal. The EM field in position space at the detector plane (i.e., $u=L_x/2$ plane) is then calculated as

$$\begin{aligned}
 E(v, z) &= \int_{-\infty}^{\infty} \int_{-\infty}^{\infty} A_d(\mathbf{k}_d) \\
 &\times \exp \left[j \left(k_{dx} \frac{L_X}{2} + k_{dy} v + k_{dz} z \right) \right] dk_{dy} dk_{dz}. \quad (11)
 \end{aligned}$$

In these derivations, the x dimension (or u dimension) of the recording slice (i.e., L_X) is not assumed to be infinite, because the variation of the height of the recording slice significantly changes the crosstalk and shift invariance, as explained in Sec. 4.

4 Performance Measures in an LHC

To compare the performance of conventional optical correlators with that of the LHC, we consider three performance measures: shift selectivity, crosstalk, and capacity. These performance measures are calculated using the theoretical derivations of Sec. 3.

In all of the simulations in this section, the recording material is assumed to be a doubly doped LiNbO₃ crystal. The images are random pixelated patterns with 20- μm pixel pitch size and it is assumed that the average of the field values is removed by dc blocking at the Fourier plane of an imaging system with unity magnification (not shown in Fig. 2). The focal length of the lens after the imaging system is 20 cm. The recording and reading wavelength is 532 nm. The thickness of each recording slice is 10 μm . The location of the recording slice Z_C is arbitrarily chosen, because according to the simulations, it has no effect on the performance measures of the LHC.

4.1 Crosstalk

Crosstalk is defined as the detected noise power in the place of a nonexistent (or empty) pattern (or hologram) produced by other stored patterns (or holograms). It is usually quan-

tified by the crosstalk noise-to-signal ratio (NSR), which is the ratio of the crosstalk noise power to the signal power diffracted from the hologram corresponding to a desired pattern. As is usual in crosstalk calculations for optical correlators, the worst-case scenario is considered for both conventional correlators and LHCs. In this scenario, it is assumed that all the recorded holograms are recorded with one pattern for all. During correlation, the holograms are read with the same pattern to maximize the unwanted crosstalk.¹⁶

In conventional holographic correlators that use the angular multiplexing method, the correlation pattern of the incoming signal beam with the stored patterns is formed at the output plane (i.e., the focal plane of a Fourier transforming lens).¹⁶ The central peaks of the correlation patterns fall at points corresponding to the reference beam angles with which the stored patterns are recorded. The sidelobes of the correlation patterns, however, may occur at the locations of the peaks of the other correlation patterns and cause crosstalk. In volume holograms, the mentioned sidelobes get suppressed as the thickness of the recording medium increases, which in turn decreases the crosstalk.¹⁶ This suppression occurs because of angular selectivity of volume holograms.¹⁵ The amount of crosstalk also depends on the examined pattern and the geometry of the correlation system, such as the focal lengths of the lenses, and the angles of the signal and the reference beams.

The reported theoretical values for crosstalk in angle multiplexed correlators in Ref. 16 indicate that for a crosstalk NSR of -30 dB in a 5-mm-thick medium the number of stored holograms can be as high as 12,000, if the material has enough dynamic range. This is obtained when the angle between the reference and the signal beams is 90 deg inside the crystal (i.e., 90-deg geometry). One can imply that for a 1-cm-thick medium, this number can be 24,000 since the width of the angular selectivity function, which is a sinc function,¹⁵ is inversely proportional to medium thickness. The acceptable crosstalk level sets a limit for the maximum number of stored patterns in an optical correlation system. This number is defined as the capacity of the correlation system.

For an LHC, we simulated the recording of holograms corresponding to identical patterns at (ξ, η) plane in successive slices of the recording medium and calculated the crosstalk NSR, produced by reading those holograms with the same pattern placed at (ξ, η) plane. Crosstalk in LHCs can be reduced by adding spacing (i.e., a buffer region) between the adjacent slices. Figure 3 shows the variation of the crosstalk NSR with this spacing. For a 1-mm-high medium (i.e., $L_X=1$ mm in Fig. 2), the curve shows that for a NSR equal to -30 dB, the corresponding spacing between adjacent slices is 13 μm . Since the thickness of each slice is 10 μm , 13+10=23 μm of the crystal length is devoted to each slice. Thus we can have 435 slices per 1 cm of crystal length. The small kinks of the curves in Fig. 3 are because of the randomness of the pixelated input patterns and are changes as the correlated patterns change.

As shown in Fig. 3, the crosstalk NSR is increased as the height of the crystal is increased. This in turn decreases the capacity of the system, as the acceptable spacing between the adjacent slices has to increase to maintain the same amount of crosstalk NSR. The reason for this variation of

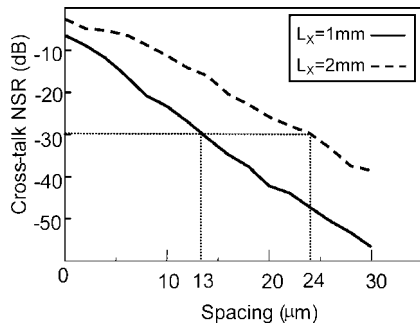


Fig. 3 Crosstalk NSR versus spacing between slices in an LHC with 1- and 2-mm-high doubly doped LiNbO_3 crystals with $10\text{-}\mu\text{m}$ -thick recording slices. Other parameters used in these simulations are $\lambda = 532\text{ nm}$ and $F = 20\text{ cm}$.

crosstalk NSR with L_X is shown in Fig. 4, which depicts the intensity profile along the z axis. It is clear from Fig. 4 that the diffracted beam becomes wider in the z direction as the height of the crystal increases, which in turn increases the crosstalk NSR. It can be shown that in the limit where the height of the crystal is infinite, the diffracted beam is a plane wave no matter how thick the slices are, and it is impossible to separate the diffracted signals coming from different slices.

A quantitative comparison of crosstalk in the two types of correlation (i.e., localized and conventional) depends on the actual design of the two systems. However, as we discuss in Sec. 4.3, crosstalk is not a limiting factor in designing conventional angle-multiplexed correlators with maximum capacity. Usually, the dynamic range limitation is the dominant effect and the crosstalk NSR obtained for the maximum capacity correlators in conventional design, is well below the required minimum value (for example, -30 dB). On the other hand, crosstalk in LHCs depends on the thickness of the buffer layer, which affects the capacity as well. For practical designs, LHCs can be designed to have crosstalk NSR below the required minimum value by choosing reasonable buffer sizes ($13\text{ }\mu\text{m}$ as mentioned).

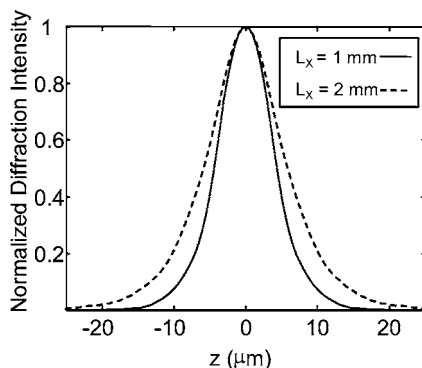


Fig. 4 Intensity profile of the diffracted beam from a single hologram in an LHC along the z axis at the bottom facets of $L_X = 1\text{ mm}$ and $L_X = 2\text{ mm}$ high LiNbO_3 crystals with $10\text{-}\mu\text{m}$ -thick recording slices. Other parameters are the same as those described in the caption of Fig. 3.

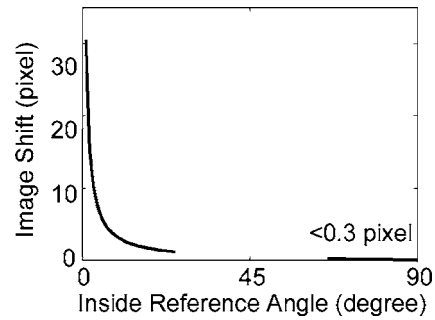


Fig. 5 In-plane shift invariance in an angle-multiplexed correlator with 1-cm-thick $\text{LiNbO}_3\text{:Fe}$ crystal with $\lambda = 532\text{ nm}$, $F = 20\text{ cm}$, and pixel pitch size $= 20\text{ }\mu\text{m}$. The two segments of the curve correspond to transmission (left) and 90-deg geometry (right) and the gap in between represents the inside angles for which no incident outside angle from air exist.

4.2 Shift Invariance

In holographic correlators, shifting the reading pattern compared to the one used in recording reduces the diffraction efficiency because of Bragg mismatch.¹⁵ The shift invariance is quantitatively defined as the minimum amount of shift required to reduce the diffraction efficiency to zero. Here we compare the shift invariance of angular multiplexed correlators and LHCs. Only in-plane shift invariance (in the x direction in Fig. 2) is considered in this comparison, because for both cases the out-of-plane shift invariance (in the y direction in Fig. 2) is more than one order of magnitude larger than the in-plane shift invariance, because of the closeness to the degeneracy direction.¹⁷

The amount of shift invariance depends on the geometry of the system and thickness of the holograms. In angular multiplexing, this thickness determines the width of the sinc function explained in Sec. 4.1, which in turn determines the shift invariance.¹⁵ The wider the sinc function, the larger is the shift invariance. On the other hand, the wider the sinc function, the larger is the crosstalk. This in turn limits the capacity of the correlator. Therefore, a trade-off exists between shift invariance and capacity. In fact, some methods such as defocusing¹⁸ have been exploited to control the shift invariance to increase the capacity of the optical correlators. Figure 5 shows shift invariance for an angular multiplexed correlator that works in the focused regime. The material is assumed to be a 1-cm-thick $\text{LiNbO}_3\text{:Fe}$ crystal. The reference beam angle with respect to the normal axis is zero and the SLM pixel pitch size is $20\text{ }\mu\text{m}$. Both transmission and 90-deg recording geometries are considered in Fig. 5. It is observed that for the 90-deg geometry, the shift-invariance is less than the size of 1 pixel.

Figure 6 shows the theoretical variation of the diffraction efficiency with image shift in an LHC. According to these simulations, the shift-invariance for an LHC with $L_X = 1\text{ mm}$ and $L_Z = 10\text{ }\mu\text{m}$ slice thickness is 5 pixels and is constant for different locations of slices within the crystal. This is better than the shift-invariance in conventional correlators, which is less than 1 pixel for 90-deg geometry, as described in the previous paragraph. As shown in Fig. 6, the shift invariance becomes smaller as the height of the crystal increases. The reason is that the diffracted beam in

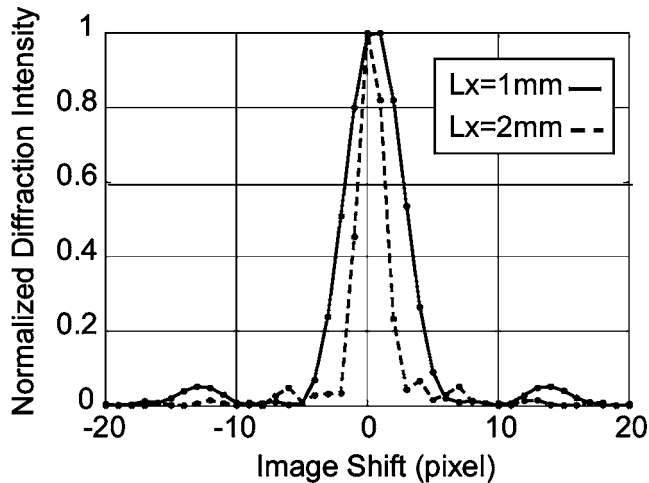


Fig. 6 Normalized diffraction efficiency versus in-plane image shift in LHCs with $L_x=1$ mm and $L_x=2$ mm high doubly-doped LiNbO_3 crystals, slice thickness= $10 \mu\text{m}$, $\lambda=532$ nm, $F=20$ cm, and pixel pitch size= $20 \mu\text{m}$.

Fig. 1(b) propagates in the x direction, resulting in a larger phase mismatch along the x direction for taller holograms (with larger L_x) for the same in-plane shift of the reading image.

4.3 Capacity

As mentioned previously, the maximum number of stored patterns in an optical correlation system defines its capacity. Here, we study the effect of diffraction efficiency (η) and dynamic range [$M/\#$ (Ref. 19)] on capacity.

For conventional angle-multiplexed holograms recorded in the same volume, it is shown that the theoretical maximum $M/\#$ for a 1-cm-thick singly doped $\text{LiNbO}_3:\text{Fe}$ crystal is 30 for transmission geometry²⁰ with recording wavelength $\lambda=514$ nm. This implies that if we choose minimum acceptable diffraction efficiency to be $\eta=10^{-4}$, the maximum number of holograms will be

$$M = \frac{M/\#}{\sqrt{\eta}} = \frac{30}{\sqrt{10^{-4}}} = 3000/\text{cm}. \quad (12)$$

In the 90-deg geometry, the theoretical maximum $M/\#$ for the same material²⁰ is 16. Thus, with the same diffraction efficiency the maximum number of holograms is 1600/cm. Comparing this number with 24,000, as calculated in Sec. 4.1, we observe that the major limit on the capacity in conventional holographic correlators is $M/\#$ and not the crosstalk.

In localized recording, we use a doubly doped $\text{LiNbO}_3:\text{Fe}:\text{Mn}$ crystal in the 90-deg geometry. The thickness of the slices and the height of the crystal are assumed to be $10 \mu\text{m}$ and 1 mm, respectively. It is shown²¹ that in this case, the maximum $M/\#$ for sensitization at 404 nm and recording at 532 nm is 0.15 (for each slice), resulting in $\eta=2.25 \times 10^{-2}$ for each hologram, which is 225 times larger than the minimum acceptable diffraction efficiency chosen in the previous paragraph for conventional correlators. This implies that we can multiplex $(225)^{1/2}=15$ holograms in a single slice with $\eta=10^{-4}$ for each hologram.

They can be exploited for different versions of a single pattern like shifted, rotated, or scaled versions. Since all these holograms correspond to the same object, they are recorded using the same reference beam in one slice. Reading the holograms with each recorded pattern (corresponding to the same object) results in diffraction of the same reference beam, which will be detected at the detector underneath the slice. This makes the LHCs much more robust to the variations of the correlated images. In addition, this capability can be exploited to develop practical 3D object recognition systems.²²

If we multiply the number of multiplexed holograms in a single slice to the maximum number of slices per 1 cm length, as calculated in Sec. 4.1, we will have $15 \times 435 = 6525$ holograms stored in a 1-cm length of doubly doped LiNbO_3 crystal (in contrast to 1600 holograms in conventional correlators with 90-deg recording geometry, as described). The result may seem surprising while the $M/\#$ of a singly doped LiNbO_3 crystal is usually larger than that of a doubly doped LiNbO_3 crystal with the same dimensions. One should notice, however, that in localized recording the diffraction efficiency of the recorded holograms is proportional to $1/M$, where M is the number of the recorded holograms.²³ The diffraction efficiency in conventional volume holography follows a $1/M^2$ dependence,²⁴ which more severely limits the number of recorded holograms. Note also that the analysis of LHCs is based on assuming 10- μm -thick slices. By using more sophisticated optics we can reduce the thickness of each slice, resulting in more independent slices to further increase the number of independent patterns recorded in the same volume.

5 Discussion

The performance characteristics of the conventional correlators and LHCs are summarized in Table 1. From Table 1, we can conclude that the LHC has better shift invariance and higher capacity while the crosstalk in both methods is comparable. Note, however, that the point of the paper is not that LHCs considerably improve the conventional performance measures. It is rather the new possibilities for obtaining practical capabilities that could not be achieved with conventional correlators. A unique property of LHCs is the possibility of erasing and rerecording in each slice without affecting other slices. Therefore, dynamic modification of the pattern database is possible. Moreover, by using long crystals ($L_z=5$ to 10 cm in Fig. 2) we can considerably increase the capacity, as shown in Fig. 7. This is not possible in conventional holography because of the absorption of the recording and reading beams through the crystal. Furthermore, the detectors in the detector array contact the bottom surface of the crystal and no lens is required to collect and focus the diffracted correlation beams in LHCs [Fig. 1(b)]. This makes the LHC a more compact system. Finally, in LHCs, patterns are recorded by gated holographic techniques, which make the holograms persistent against further reading.

6 Conclusion

In this paper, we demonstrated the LHC as an optical correlation system with which one can dynamically record and erase individual patterns in the recording medium without disturbing other stored patterns. We showed that LHCs

Table 1 Performance characteristics of conventional correlators and localized correlators.

Method	Shift Invariance	Crosstalk (NSR)	Capacity per Centimeter of Thickness	Size	Selective Recoding/Erasure	Elongation Possibility
Conventional (angular—90 deg)	<1 pixel	<-30 dB	1600	Large	No	No
Localized	5 pixels	<-30 dB	6525 (in 435 groups)	Compact	Yes	Yes

The holograms are persistent in LHCs.

have better performance than conventional volume holographic optical correlators in terms of shift invariance, crosstalk, and capacity. Moreover, the LHC is more compact and its capacity can be extended by elongating the recording medium. The LHCs can also be used to improve the properties of 3-D optical correlators.

7 Appendix: Derivation of Fresnel Diffraction Formula

In this appendix we derive the Fresnel diffraction formula that relates the EM field within the recording slice volume [i.e., $F(u, v, z)$] to that at the SLM plane [i.e., $f(\xi, \eta)$] in Fig. 2. For the simplicity of deriving the diffraction pattern in the recording medium, the front face of the recording medium is assumed to be at the Fourier plane of the lens. Because the height of the recording medium (L_x) in LHCs is relatively small (about 1 mm), it is also important to couple most of the signal beam into the recording medium. Therefore, focusing the signal beam at the entrance of the recording medium is useful in that way as well. The EM field at the back focal plane of the lens ($z=0$) is

$$H(x, y) \propto \text{FT}\{f(\xi, \eta)\} = G\left(\frac{x}{\lambda F}, \frac{y}{\lambda F}\right), \tag{13}$$

where FT represents Fourier transformation, and the Fourier transform of the function f is represented by the function G . Light propagates through the crystal with average refraction index of n . We use Fresnel diffraction approximation to evaluate the EM field at any location within the recording medium with longitudinal distance z to the back focal plane of the lens. Moreover, we assume the reflection coefficients at the boundary between air and the recording medium to be constant within the whole spatial frequency spectrum of the signal beam. Assuming paraxial approximation and using the kernel of the Fresnel diffraction,²⁵ we obtain

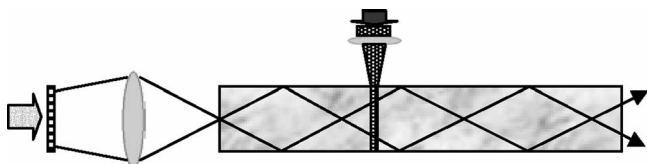


Fig. 7 Index waveguiding in localized holographic correlator with long crystals to increase capacity.

$$\begin{aligned}
 F(u, v, z) &\propto \left\{ H(x, y) ** \frac{1}{j\lambda z} \exp\left(j\frac{2\pi n z}{\lambda}\right) \right. \\
 &\quad \left. \times \exp\left[j\frac{n\pi}{\lambda z}(x^2 + y^2)\right] \right\} \\
 &= \left\{ G\left(\frac{x}{\lambda F}, \frac{y}{\lambda F}\right) ** \frac{1}{j\lambda z} \exp\left(j\frac{2\pi n z}{\lambda}\right) \right. \\
 &\quad \left. \times \exp\left[j\frac{n\pi}{\lambda z}(x^2 + y^2)\right] \right\} = \text{FT}^{-1}\left\{ f(-\xi, -\eta) \right. \\
 &\quad \left. \times \exp\left[-j\frac{\pi z}{n\lambda F^2}(\xi^2 + \eta^2)\right] \right\} \frac{1}{j\lambda} \\
 &\quad \times \exp\left(j\frac{2\pi n z}{\lambda}\right), \tag{14}
 \end{aligned}$$

where ** stands for 2-D convolution and FT^{-1} represents inverse Fourier transformation. Rewriting the FT^{-1} in its integral form and omitting the constant term of $1/j\lambda$ yields

$$\begin{aligned}
 F(u, v, z) &\propto \int \int_{\text{SLM}} f(-\xi, -\eta) \exp\left[-j\frac{\pi z}{n\lambda F^2}(\xi^2 + \eta^2)\right] \\
 &\quad \times \exp\left(j\frac{2\pi n z}{\lambda}\right) \exp\left[j\frac{2\pi}{\lambda F}(u\xi + v\eta)\right] d\xi d\eta. \tag{15}
 \end{aligned}$$

By negating the variables ξ and η , the final form of the EM field within the recorded slice is obtained

$$\begin{aligned}
 F(u, v, z) &\propto \int \int_{\text{SLM}} f(\xi, \eta) \exp\left[-j\frac{\pi z}{n\lambda F^2}(\xi^2 + \eta^2)\right] \\
 &\quad \times \exp\left(j\frac{2\pi n z}{\lambda}\right) \exp\left[-j\frac{2\pi}{\lambda F}(u\xi + v\eta)\right] d\xi d\eta. \tag{16}
 \end{aligned}$$

Acknowledgments

This work was supported by Air Force Office of Scientific Research (G. Pomrenke) and by Georgia Electronic Design Center (GEDC). The authors would like to thank Babak Momeni for useful discussions.

References

1. A. B. VanderLugt, "Signal detection by complex spatial filtering," *IEEE Trans. Inf. Theory* **IT-10**(2), 139–148 (1964).
2. C. S. Weaver and J. W. Goodman, "A technique for optically convolving two functions," *Appl. Opt.* **5**(7), 248–249 (1966).
3. P. J. van Heerden, "Theory of optical information storage in solids," *Appl. Opt.* **2**(4), 393–400 (1963).
4. D. Psaltis and F. Mok, "Holographic memory," *Sci. Am.* **273**(5), 70–76 (1995).
5. D. Psaltis, D. Brady, X. G. Gu, and S. Lin, "Holographic in artificial neural networks," *Nature (London)* **343**(6256), 325–330 (1990).
6. A. Pu, R. Denkewalter, and D. Psaltis, "Real-time vehicle navigation using a holographic memory," *Opt. Eng.* **36**(10), 2737–2746 (1997).
7. G. W. Burr, S. Kobras, H. Haussen, and H. Coufal, "Content-addressable data storage using volume holograms," *Appl. Opt.* **38**(32), 6779–6784 (1999).
8. G. R. Mangasaryan, B. E. Khaikin, and V. S. Khitrova, "Matched filtering on basis of thick holograms for fingerprint identification," *Opt. Commun.* **22**(2), 169–172 (1977).
9. C. Moser, B. Schupp, and D. Psaltis, "Localized holographic recording in doubly doped lithium niobate," *Opt. Lett.* **25**(17), 162–164 (2000).
10. O. Momtahan, A. Karbaschi, and A. Adibi, "Gated holography: materials, techniques, and applications," *Proc. SPIE* **4988**, 24–39 (2003).
11. G. W. Burr, F. H. Mok, and D. Psaltis, "Angle and space multiplexed holographic storage using the 90-degree geometry," *Opt. Commun.* **117**(1–2), 49–55 (1995).
12. D. von der Linde, A. M. Glass, and K. F. Rodgers, "Multiphoton photorefractive process for optical storage in LiNbO₃," *Appl. Phys. Lett.* **25**(3), 155–157 (1974).
13. K. Buse, A. Adibi, and D. Psaltis, "Non-volatile holographic recording in doubly doped lithium niobate crystals," *Nature (London)* **393**(6686), 665–668 (1998).
14. A. Adibi, K. Buse, and D. Psaltis, "Two-center holographic recording," *J. Opt. Soc. Am. B* **18**(5), 584–601 (2001).
15. H. J. Coufal, D. Psaltis, and G. T. Sincerbox, Eds., *Holographic Data Storage*, Springer-Verlag, Berlin (2000).
16. C. Gu, H. Fu, and J. R. Lien, "Correlation patterns and cross-talk noise in volume holographic optical correlators," *J. Opt. Soc. Am. A* **12**(5), 861–868 (1995).
17. C. Gu, J. Hong, and S. Campbell, "2-D shift-invariant volume holographic correlator," *Opt. Commun.* **88**(4–6), 309–314 (1992).
18. M. Levene, G. J. Steckman, and D. Psaltis, "Method for controlling the shift invariance of optical correlators," *Appl. Opt.* **38**(2), 394–398 (1999).
19. F. H. Mok, G. W. Burr, and D. Psaltis, "System metric for holographic memory systems," *Opt. Lett.* **21**(12), 896–898 (1996).
20. K. Buse and E. Krätzig, "Inorganic photorefractive materials," in *Holographic Data Storage*, H. J. Coufal, D. Psaltis, G. T. Sincerbox, Eds., pp. 113–125, Springer-Verlag, Berlin (2000).
21. O. Momtahan and A. Adibi, "Global optimization of sensitivity and dynamic range for two-center holographic recording," *J. Opt. Soc. Am. B* **20**(3), 449–461 (2003).
22. S.-H. Shin and B. Javidi, "Three-dimensional object recognition by use of a photorefractive volume holographic processor," *Opt. Lett.* **26**(15), 1161–1163 (2001).
23. C. Moser, I. Maravic, B. Schupp, A. Adibi, and D. Psaltis, "Diffraction efficiency of localized holograms in doubly doped LiNbO₃ crystals," *Opt. Lett.* **25**(17), 1243–1245 (2000).
24. D. Psaltis, D. Brady, and K. Wagner, "Adaptive optical networks using photorefractive crystals," *Appl. Opt.* **27**(9), 1752–1759 (1988).
25. J. W. Goodman, *Introduction to Fourier Optics*, McGraw-Hill, New York (1996).



Arash Karbaschi was a member of the National Physics Olympiad team in 1992. He received his BSc degree in 1995 and his MSc degree in 1997 in electrical engineering from Sharif University of Technology, Tehran, Iran. In 2001 he moved to the United States and has since been a PhD student in electrical engineering at the Georgia Institute of Technology. His research area is applications of holography in pattern recognition, biosensing, and rapid prototyping.



Omid Momtahan was a member of the Iranian Physics Olympiad Team in 1992, participating in the 23rd International Competitions in Helsinki, Finland. He received a BS degree in electrical engineering from the University of Shiraz in 1996, ranking first among his graduating class. He was with the Electrical Engineering Department of Sharif University of Technology from 1996, and received his MS degree in 1998. He is currently a PhD student at the School of Electrical and Computer Engineering, Georgia Institute of Technology. He received the best paper award at the 50th IEEE Vehicular Technology Conference held in Amsterdam, the Netherlands, in September 1999. His research interests are volume holographic memories, optical communications, and wireless communications.



Ali Adibi was born in Shiraz, Iran, in 1967. He received his BSEE degree from Shiraz University, in 1990, his MSEE degree from the Georgia Institute of Technology, Atlanta, in 1994, and his PhD degree from the California Institute of Technology, Pasadena, in 1999. His PhD research resulted in a breakthrough in persistent holographic storage in photorefractive crystals. He was a postdoctoral scholar at California Institute of Technology from 1999 to 2000. He has been an assistant professor in the School of Electrical and Computer Engineering, Georgia Institute of Technology, since 2000. His research interests include holographic data storage, holographic optical elements for optical communications, 3-D optical pattern recognition, design, characterization, and applications of photonic crystals for chip-scale wavelength-division multiplexing (WDM) and biosensors, and optical communication and networking. He is a member of Sigma Xi, OSA, SPIE, and the Materials Information Society (ASM).



Bahram Javidi is a Board of Trustees Distinguished Professor of Electrical and Computer Engineering at the University of Connecticut. Dr. Javidi is a fellow of the IEEE, the OSA, and the SPIE. He received the IEEE Lasers and Electro-optics Society Distinguished Lecturer Award in 2003, the IEEE Best Journal Paper Award from *IEEE Transactions on Vehicular Technology* in 2002, and from the University of Connecticut, the Alumni Association Excellence in Research Award, the Chancellor's Research Excellence Award, and the first Electrical and Computer Engineering Department Outstanding Research Award. He published the books *Optical and Digital Techniques for Information Security* (Springer, 2003), *Image Recognition: Algorithms, Systems, and Applications* (Marcel Dekker, 2002); *Three Dimensional Television, Video, and Display Technologies* (Springer Verlag, 2002); *Smart Imaging Systems* (SPIE Press, 2001); *Real-time Optical Information Processing* (Academic Press, 1994); and *Optical Pattern Recognition* (SPIE Press, 1994). He has published over 170 technical papers in major journals. Dr. Javidi received his BS degree in electrical engineering from George Washington University and his MS and PhD degrees in electrical engineering from the Pennsylvania State University.